Photo-assisted electron emission from illuminated monolayer graphene

M. Upadhyay Kahaly,[1] Shikha Misra,[2,3,a)] and S. K. Mishra[1]
[1]*ELI-ALPS, Szeged, Hungary*
[2]*Centre for Energy Studies (CES), Indian Institute of Technology Delhi (IITD), New Delhi, India*
[3]*F-32, CSIR-CEERI Col. Pilani, India*

(Received 30 March 2017; accepted 16 May 2017; published online 31 May 2017)

We establish a formalism to address co-existing and complementing thermionic and photoelectric emission from a monolayer graphene sheet illuminated via monochromatic laser radiation and operating at a finite temperature. Taking into account the two dimensional Fermi-Dirac statistics as is applicable for a graphene sheet, the electron energy redistribution due to thermal agitation via laser irradiation, and Fowler's approach of the electron emission, along with Born's approximation to evaluate the tunneling probability, the expressions for the photoelectric and thermionic emission flux have been derived. The cumulative emission flux is observed to be sensitive to the parametric tuning of the laser and material specifications. Based on the parametric analysis, the photoemission flux is noticed to dominate over its coexisting counterpart thermionic emission flux for smaller values of the material work function, surface temperature, and laser wavelength; the analytical estimates are in reasonably good agreement with the recent experimental observations [Massicotte *et al.*, Nat. Commun. **7**, 12174 (2016)]. The results evince the efficient utilization of a graphene layer as a photo-thermionic emitter. *Published by AIP Publishing.*
[http://dx.doi.org/10.1063/1.4984318]

I. INTRODUCTION AND MOTIVATION

Since the advent of the thermionic energy converter (TEC) concept, a considerable effort has been devoted to enhancing current densities/charged flux between electrodes;[1,2] such investigations[3–6] have been of significance in the continuous development of power plants as an alternative energy source and numerous space applications, in particular, generating autonomous power in deep space assets.[5,6] An innovative notion for the current enhancement is proposed by Smestad[7] and Shwede *et al.*[8] where the electron population over the Fermi level inside a p-type semiconductor material is modified via laser illumination of its surface.

The invention of advanced materials such as graphene (2D honeycomb allotrope of carbon[9,10]) has added a novel aspect in achieving significant current and efficient energy conversion; the ultrahigh electrical conductivity/mobility associated with graphene is attributed to the availability of free electrons in the linear band structure in the proximity of the Fermi level.[11,12] In a recent experimental work,[13] a prominent photo-thermionic emission current is measured from infrared laser irradiated graphene based heterostructures. The enhanced current is instigated by the redistribution of the photo assisted charge carriers at higher energy levels (in the form of hot electrons) over the Fermi energy. This effect of photo-thermionic current has qualitatively been discussed by introducing an arbitrary increase in the Fermi level (i.e., reducing Schottky barrier). Taking concern of the unique optical properties of graphene (or graphene based structures[12]) such as broadband absorption,[14] ultrafast response,[15] and gate-tunability,[16] recent investigations (Ref. 13 and references therein) suggest the possibility of graphene to demonstrate the photon-assisted thermionic emission, as required in fabricating efficient photovoltaic cells/photo-detectors. The slow rate electron lattice cooling process[17] and intra-band Auger type scattering[18] allowing strong thermionic flux and efficient laser absorption by ambient carriers, respectively, in graphene, make it an adequate choice for the generation of significant charge carriers and hence enhanced current.

The laser illumination might induce both the thermionic and photoelectric effects simultaneously in order to liberate electrons from a 2D graphene sheet. In order to address the phenomenon of photo-assisted electron emission, in this work, a formalism describing the electron emission flux through laser irradiated suspended monolayer graphene has been established. The formulation takes into account 2D Fermi-Dirac (*f-d*) statistics[19] applicable in the case of the monolayer graphene sheet for the evaluation of the density of states and Fowler's treatment[20] of the electron emission. Consequently, the expressions for the thermionic and photoelectric emission currents for the positively/negatively charged 2D surfaces have been derived. On the basis of the present analysis, a significant enhancement in the electron emission flux due to laser illumination is predicted and illustrated graphically; the effect is anticipated to be more pronounced for the surfaces with a high temperature and low work function material. The evaluation of the electron emission current from the laser radiated infinitesimal thin 2D sheet (later applied to the monolayer graphene) along with the inherent mechanisms has been analyzed in Sec. II. The parameters relevant to graphene and corresponding numerical results based on the parametric analysis along with physical interpretation have been discussed in Sec. III. A summary of the outcome from this analysis in Sec. IV concludes this paper.

[a)]E-mail: shikhamish@gmail.com

II. ELECTRON EMISSION FROM AN INFINITESIMAL THIN SHEET (MONOATOMIC GRAPHENE LAYER)

According to Wallace's theory[21] for graphene like fine structures, the electrons in the thin sheet exhibit Fermionic character and follow Fermi-Dirac statistics inside the sheet. In this 2D sheet (say the yz plane) framework, the electrons are in the low energy quantum regime[22] with a quantized parallel energy $E_t = \hbar v_f k_t$, where v_f refers to the velocity of massless Dirac fermions in graphene; this dispersion relation also infers the E-k diagram for graphene. Thus, the number of electronic states per unit cell of energy lying between E_t and (E_t+dE_t)can be written as[23,24]

$$\rho(E_t)dE_t = \left[2/(2\pi)^2\right]dk_y dk_z = \left[2/(2\pi)^2\right]2\pi k_t dk_t = \left[1/\pi(\hbar v_f)^2\right]E_t dE_t. \tag{1a}$$

Thus, the number of electrons hitting the top layer (available for emission) from inside, having the total energy between E and $(E+dE)$ and normal energy (assuming $\hat{x}$ to be normal to the planar surface) between E_x and (E_x+dE_x), can be written as[25]

$$\begin{aligned} n_{e,fd}(E,E_x)dEdE_x &= \left[1/\pi(\hbar v_f)^2\right]E_t(2mE_x)^{1/2}f_{de}(E)dE_x dE \\ &\Rightarrow n_{e,fd}(\varepsilon,\varepsilon_x)d\varepsilon d\varepsilon_x \\ &= (\beta_0/e)T^3(m/2kT)^{1/2}\varepsilon_x^{-1/2} \\ &\quad\times(\varepsilon-\varepsilon_x)f_{de}(\varepsilon)d\varepsilon d\varepsilon_x, \end{aligned} \tag{1b}$$

where $\beta_0 = (ek^3/\pi\hbar^3 v_f^2)$, $f_{de}(\varepsilon) = [1+\exp(\varepsilon-\varepsilon_f)]^{-1}$ refers to Fermi-Dirac distribution,[19] m is the electronic mass, $\varepsilon_x = E_x/kT = \hbar^2k_x^2/2mkT$, $\varepsilon_f = E_f/kT$, E_f refers to intrinsic Fermi energy level relative to the Dirac point, $\hbar$ and k correspond to reduced Planck's and Boltzmann's constants, respectively, and T is the absolute temperature of the electron emitting surface. For the monolayer graphene sheet[26] $v_f = 1.1\times10^6$m/s, $\beta_0 \sim 92$A/m^{2}K^3, and intrinsic Fermi level $E_f \sim 0.055$ eV (at $\sim$300 K) with its linear temperature dependence (as $E_f \propto T$, Ref. 27) are taken into account for the calculations.

The momentum distribution of electrons, impinging the top layer surface $(x=0)$ from inside having the total energy between ε and $(\varepsilon+d\varepsilon)$ and normal energy between ε_x and $(\varepsilon_x+d\varepsilon_x)$, per unit area per unit time, can be written as[25]

$$\begin{aligned} n_{1,fd}(\varepsilon,\varepsilon_x)d\varepsilon d\varepsilon_x &= (2kT\varepsilon_x/m)^{1/2}n_{e,fd}(\varepsilon,\varepsilon_x)d\varepsilon d\varepsilon_x \\ &= (\beta_0/e)T^3(\varepsilon-\varepsilon_x)f_{de}(\varepsilon)d\varepsilon d\varepsilon_x. \end{aligned} \tag{2a}$$

The integration of the above expression within suitable limits over the surface barrier $(0, w_a)$ refers to the total number of electrons available (n_t) for the emission where $w_a(=eW_a/kT)$ refers to the surface barrier height. Consider that the sheet is illuminated by a monochromatic laser source. A fraction (say α) of the incident photon flux (effective flux $I_o = \alpha I_{in}$) interacts with the $\kappa\Lambda$ fraction of the electrons hitting the top layer from inside,[20] which is utilized in the emission (via photoemission/tunneling[28]) of the electrons and increase in the surface temperature; here, κ infers the probability per unit time of absorption of an incident photon per unit area per unit time by an electron hitting normally the top layer from inside, Λ refers to the photon flux responsible for electron emission, and I_{in} may be correlated with incident laser power P_L over a spot size σ_s as $P_L = \sigma_s I_{in}$. A finite fraction (say η) of the energized electrons involves in the electron-phonon interaction, resulting in an enhanced surface (and bulk) temperature. Following the energy balance over the surface,[13] the increase in surface temperature may be expressed as $\delta T = (\eta I_o/D\Gamma)$, resulting in effective surface temperature $T = (T_o + \delta T)$; here, D and Γ refer to the duty cycle of the laser and the thermal lattice conductance, respectively. In a recent work, the monolayer graphene[13] is shown to be characterized by parameters $\alpha = 0.5\%$, $\eta = 70\%$, $D \sim 0.4\%$, and $\Gamma \sim (0.5\pm0.3)$MW/m^{2}K. The increase in surface (or bulk) temperature leads to the redistribution of the electrons in the available high energy states. The fraction $f_t \equiv 1-(1-\eta)\kappa\Lambda$ of the electrons (effectively at temperature T) hitting the top layer from inside contributes to usual thermionic emission (for $\varepsilon_x > w_a$) and quantum tunneling emission (for $\varepsilon_x \le w_a$). The momentum distribution associated with these electrons inside sheet can be expressed as[25]

$$n_{1,th}(\varepsilon,\varepsilon_x)d\varepsilon d\varepsilon_x = f_t(\beta_0/e)T^3(\varepsilon-\varepsilon_x)f_{de}(\varepsilon)d\varepsilon d\varepsilon_x, \tag{2b}$$

$$n_{1,th}(\varepsilon_x)d\varepsilon_x = f_t(\beta_0/e)T^3\left(\int_{\varepsilon_x}^{\infty}(\varepsilon-\varepsilon_x)f_{de}(\varepsilon)d\varepsilon\right)d\varepsilon_x, \tag{2c}$$

$$= f_t(\beta_0/e)T^3\left(\int_0^{\infty}\varepsilon f_{de}(\varepsilon+\varepsilon_x)d\varepsilon\right)d\varepsilon_x. \tag{2d}$$

Using f-d statistics for the electrons inside the sheet, the normal distribution can be formatted as

$$n_{1,t}(\varepsilon_x)d\varepsilon_x = f_t(\beta_0/e)T^3\left[-\text{Polylog}\left[2,-\exp\left[-(\varepsilon_x-\varepsilon_f)\right]\right]\right]d\varepsilon_x. \tag{3}$$

The notation Polylog $[u, v]$ in the above expression corresponds to the polylogarithm function and can be expressed as power series: $Li_u(v) = \sum_{l=1}^{\infty}(v^k/k^u)$.

The flux coming out due to the thermionic emission can be obtained by integrating the above expression [Eq. (3)] over the surface potential barrier. If the graphene surface is at finite negative potential $(V_s < 0)$, the electrons may also tunnel through the potential barrier for the normal energy $(w_a - v_s) \le \varepsilon_x \le w_a$ with finite probability $T(\varepsilon_x)$, resulting in field emission, while for the energy $\varepsilon_x > w_a$, the electrons exhibit thermionic emission (with $T(\varepsilon_x) \sim 1$); here, $v_s = -(eV_s/kT)$. In the case of the surface at positive potential (i.e., $V_s \ge 0$), the electrons exhibit only thermionic emission for the normal energy $\varepsilon_x > (w_a - v_s)$. The thermionic flux in this case can be written as[28–30]

$$n_{th} = \int_{w_a-v_s,0}^{w_a}T(\varepsilon_x)n_{1,t}(\varepsilon_x)d\varepsilon_x + \int_{w_a}^{\infty}n_{1,t}(\varepsilon_x)d\varepsilon_x \quad \text{for } v_s \ge 0, \tag{4a}$$

$$= \int_{w_a-v_s}^{\infty}n_{1,t}(\varepsilon_x)d\varepsilon_x \quad \text{for } v_s < 0. \tag{4b}$$

The thermionic flux from the uncharged surface can be obtained by putting $v_s = 0$ in the above expression, and this can be expressed as

$$n_{th0} = f_t(\beta_0/e)T^3 \int_{w_a}^{\infty} \left[-\text{Polylog}\left[2, -\exp\left[-(\varepsilon_x - \varepsilon_f)\right]\right]\right] d\varepsilon_x. \tag{4c}$$

Remaining electron population (i.e., $f_p \equiv (1-\eta)\kappa\Lambda$) causes the photoemission[30] for the normal energy $\varepsilon_x + \varepsilon_\nu > w_a$, while for the energy range, $\varepsilon_x + \varepsilon_\nu \leq w_a$ corresponds to light induced field emission. The momentum distribution of the electrons after absorbing a photon with photo-enhanced normal energy ($\varepsilon_\nu = h\nu/kT$) can be obtained by replacing $\varepsilon' = \varepsilon + \varepsilon_\nu$ and $\varepsilon'_x = \varepsilon_x + \varepsilon_\nu$ in Eqs. (2a) and (2b) and can be written as

$$n_{1,ph}(\varepsilon, \varepsilon_x) d\varepsilon d\varepsilon_x = f_p(\beta_0/e)T^3(\varepsilon - \varepsilon_x) f_{de}(\varepsilon - \varepsilon_\nu) d\varepsilon d\varepsilon_x, \tag{5a}$$

$$n_{1,ph}(\varepsilon_x) d\varepsilon_x = f_p(\beta_0/e)T^3 \left(\int_0^{\infty} \varepsilon f_{de}(\varepsilon + \varepsilon_x - \varepsilon_\nu) d\varepsilon \right) d\varepsilon_x. \tag{5b}$$

In writing the above equation [Eq. (5)], the primes are omitted. Note that in the formulation, the energy levels in the distribution are measured from the bottom of the conduction band, and the energy of the electrons at this level is referred to as zero. Using *f-d* statistics for the electrons inside the sheet, the normal distribution in this case may be formatted as[31,32]

$$n_{1,p}(\varepsilon_x) d\varepsilon_x = f_p(\beta_0/e)T^3 \left[-\text{Polylog} \times \left[2, -\exp\left[-(\varepsilon_x - \varepsilon_\nu - \varepsilon_f)\right]\right]\right] d\varepsilon_x. \tag{6}$$

Similar to the previous case, the net flux associated with the photoelectrons can be written as

$$n_{ph} = \int_{w_a - \upsilon_s, 0}^{w_a} T(\varepsilon_x) n_{1,p}(\varepsilon_x) d\varepsilon_x + \int_{w_a}^{\infty} n_{1,p}(\varepsilon_x) d\varepsilon_x \quad \text{for } \upsilon_s \geq 0, \tag{7a}$$

$$= \int_{w_a - \upsilon_s}^{\infty} n_{1,ph}(\varepsilon_x) d\varepsilon_x \quad \text{for } \upsilon_s < 0. \tag{7b}$$

Again, the photoemission flux coming out from the uncharged surface can be written as

$$n_{ph0} = f_p(\beta_0/e)T^3 \int_{w_a}^{\infty} \left[-\text{Polylog}\left[2, -\exp\left[-(\varepsilon_x - \varepsilon_\nu - \varepsilon_f)\right]\right]\right] d\varepsilon_x. \tag{7c}$$

For the sake of simplicity of the analysis, we use the expression based on Born's approximation[33,34] to evaluate the tunneling probability as

$$T(\varepsilon_x) = \exp\left[-(4\beta_s/3\upsilon_s)(w_a - \varepsilon_x)^{3/2}\right], \tag{8}$$

where $\beta_s = (2m_e kTs^2/\hbar^2)^{1/2}$, while s infers the strength of the electric field for surface potential V_s and corresponds to its extension normal to the surface.

Another crucial parameter in the formulation is κ, which effectively leads to the redistribution of the electrons to the higher energy states causing enhanced electron emission from thermionic and photoelectric effects. For the known surface parameters, this parameter κ can be determined by equating the factor $\kappa\Lambda$ of the total electrons available for the emission with absorbed incident photon flux as $\kappa\Lambda n_t = (I_o/\varepsilon_\nu) \Rightarrow \kappa n_t = 1$.

III. NUMERICAL RESULTS AND DISCUSSION

From the above expressions obtained in the analysis, the emission current [see Eqs. (4) and (7)] is noticed to be a function of independent parameters T (or δT), s, barrier height w_a, surface potential υ_s, and incident photon energy ε_ν. The incident laser radiation comes into picture in determining the parameter T ($=T_o+\delta T$), photon flux (Λ), ε_ν, and κ in assistance with other material properties. Further considering the emitting surface as a monolayer graphene structure, the barrier height of the quantum well (corresponding to the Dirac point) may be taken equivalent to the inherent work function (φ) of the bulk material, which can be tuned to a wide range via the surface morphology/engineering. In general, the graphene structure is grown over various substrates [such as SiC, Ir (111), Ge (100)/Si (100), and Ru (0001)] and in different possible orientations.[35] The substrate interaction with adjacent graphene affects its work function and hence the electron emission flux. The variation in the work function depends on the binding strength of graphene with the substrate.[35] For instance, in a high temperature regime, the strong binding between graphene and Ru (0001) yields a remarkably low work function (3.3 ± 0.1 V), whereas due to a relatively weak interaction, graphene grown on Ir (111) displays a larger thermionic work function ($\sim$4.4 V);[35] moreover, the work function is also noticed to be sensitive to the in-plane orientation of the graphene. In a recent work,[13] this is noticed to acquire as low as $\varphi \sim 0.6$ V for the graphene/WSe_2 interface; although this value is far from pristine graphene, note that the defects that are inevitable in experimental synthesis can induce carriers and may result in such a substantial change in the work function (φ). In our analysis, we have parametrically examined the influence of varying work functions of tuned graphene on the emission current, which apparently infers the effect of substrates. Further, for the sake of simplicity in the analytical calculations, the laser radiation is considered monochromatic in nature; however, a similar approach is applicable in the case of a broad continuous spectrum, and emission current may be obtained by integrating Eqs. (4) and (7) over the entire frequency spectrum.[28]

In order to have a notion of the magnitude of the coexisting flux (i.e., currents) associated with the thermionic and photoelectric effects, respective dimensionless parameters $C_{th0}[= n_{th0}/f_t(\beta_0/e)T^3]$ and $C_{ph0}[= n_{ph0}/f_p(\beta_0/e)T^3]$ corresponding to an uncharged surface ($\upsilon_s = 0$) have been illustrated as a function of $(w_a - \varepsilon_f)$ in Figs. 1(a) and 1(b). The thermionic flux [C_{th0}, Fig. 1(a)] decreases with an increase in $(w_a - \varepsilon_f)$, which can be understood in terms of a decrease in the electron population available for emission with an increase in the barrier height of the quantum well. The effect of energy of the incident photon (ε_ν) on the photoemission flux from the uncharged surface is displayed in Fig. 1(b). The emission flux is noticed to increase with increasing photon energy; this may be attributed to the higher electron

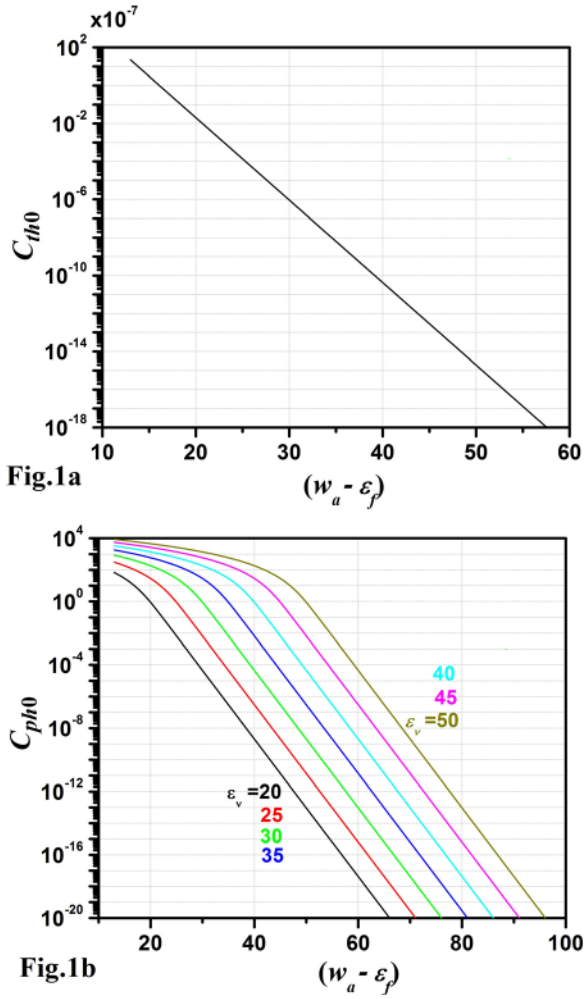

FIG. 1. The electron emission flux from the uncharged graphene sheet corresponding to (a) thermionic (C_{th0}) and (*b*) photoelectric (C_{ph0}) effects as a function of $(w_a - \varepsilon_f)$; the color labels of the varying parameter ε_ν in (b) are indicated on the curves.

population available for emission over the barrier height (i.e., the energy range ϵ (W_a, ∞)), with increasing photon energy (ε_ν). These curves may be used to estimate the numerical value of the emission current by using the appropriate values of the laser and graphene parameters. For example, typical parameters mentioned above for graphene (*viz.*, $\alpha = 0.5\%$, $\eta = 70\%$, $D \sim 0.4\%$, $\Gamma \sim 0.5\text{MW/m}^2\text{K}$, $E_f = 0.055\text{eV}$ at 300 K, and $\varphi \sim 1.0\text{eV}$) along with the laser radiation parameters (i.e., $\lambda \sim 1.5\mu\text{m}$, $I_{in} \sim 4 \times 10^3\text{Wcm}^{-2}$, and $\Lambda \sim 1.5 \times 10^{20}\text{cm}^{-2}$) cause an increase in the surface temperature $\delta T = 70\text{K}$. Taking the background (surrounding) temperature $T_o = 400\text{K}$, one gets $w_a - \varepsilon_f \approx 22.5$, $\kappa \sim 2.65 \times 10^{-26}\text{cm}^2$, and $\varepsilon_\nu \approx 20.6$; in terms of the emission current, these data correspond to $\sim$1.8 Am^{-2} (thermionic) and $\sim$1248 Am^{-2} (photoelectric). If one assumes that the surface area available for the emission is equal to the spot size of the laser ($\sim$2.5 μm^2), the net current coming out from an uncharged surface is $\sim$0.005 nA and $\sim$3.1 nA, respectively; for this particular case, the photoemission flux is noticed higher by three orders of the magnitude than the thermionic flux.

After obtaining the current estimate from the uncharged surface, we next perform the parametric analysis of the thermionic and photoelectric flux. The ratio of the emission flux from the surface at finite potential to the flux from the uncharged surface ($R_{th} = n_{th}/n_{th0}$ and $R_{ph} = n_{ph}/n_{ph0}$) using equations [Eqs. (4) and (7)] as a function of different physical variables has been illustrated in Figs. 2–5. The parametric study has been made for the following set of standard parameters for graphene, while the effect of individual parameters on the current ratio has been evaluated by varying it over a wide range and keeping others the same. $T_o = 400\,\text{K}$, $(1-\eta)\alpha I_{in} = (1-\eta)I_o = 4 \times 10^{19}\,\text{Wcm}^{-2}$, $\lambda = 1500\,\text{nm}$, $h\nu = 0.78\,\text{eV}$, $s = 0.1\,\mu\text{m}$, $\varphi \sim 4.7\,\text{eV}$, and $E_f = 0.055\,\text{eV}$ at 300 K. It should also be mentioned here that although the calculations have been performed for this particular set of parameters for the pristine monolayer graphene, the present formulation is well applicable to any arbitrary material sheet/parameters.

Under a monochromatic laser illumination and operating at a finite temperature, the monolayer graphene sheet may acquire finite positive or negative potential depending on the dominance of electron emission and accretion of plasma particles over its surface. Hence, it is of interest to estimate the

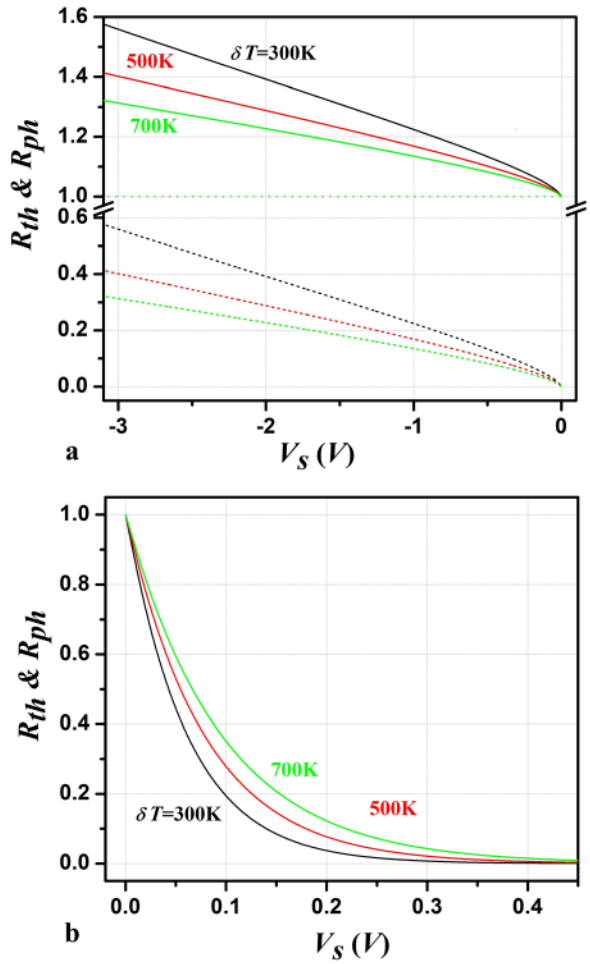

FIG. 2. The ratio of currents (R_{th} and R_{ph}) as a function of surface potential from the graphene sheet corresponding to (a) $V_s \leq 0$ and (b) $V_s \geq 0$ for different values of δT and the standard set of parameters stated in the text. In (a), the broken, dotted, and solid curves refer to field emission, usual emission, and total flux associated with negatively charged surfaces, respectively, while the color labels of the varying parameter δT is indicated on the curves of the figure.

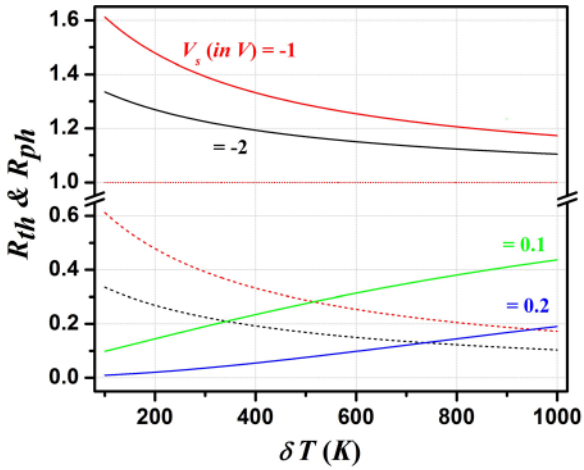

FIG. 3. The ratio of currents (R_{th} and R_{ph}) as a function of the parameter δT from graphene sheet for different values of V_s and standard set of parameters stated in the text. In figure the broken, dotted and solid curves refer to field emission, usual emission and total flux, respectively, while the color labels of the varying parameter V_s are indicated on the curves.

influence of surface potential on the emission flux. The dependence of the current ratios (R_{th} and R_{ph}) on the surface potential for different values of parameter δT has been illustrated in Fig. 2. It is interesting to note from our calculations that the ratio of two cases are found to be nearly the same, i.e., $R_{th} \approx R_{ph}$ for the parameters considered herein; however, the current magnitudes are significantly different. It should also be noted that emission current through tunneling [field emission, 1st term in Eqs. (4a) and (7a)] occurs only when the surface potential is negative, while the usual emission (2nd term) is independent of surface potential for $V_s < 0$. The field emission and usual emission flux are shown by broken and dotted lines in the figure, while the solid line corresponds to the total emission flux. The field emission current is noticed to increase with increasing

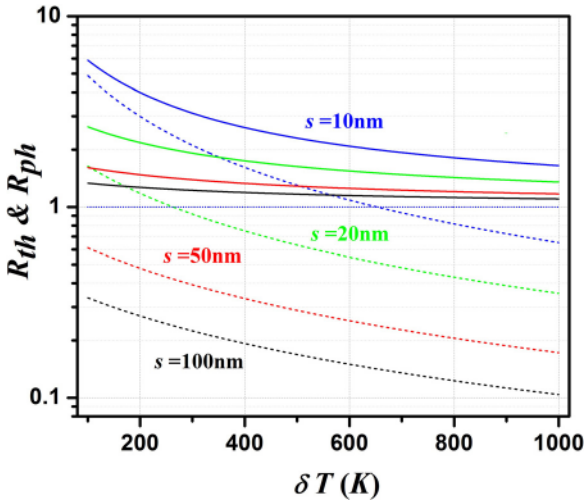

FIG. 4. The ratio of currents (R_{th} and R_{ph}) as a function of the parameter δT from the graphene sheet for different values of parameter s defining the field strength for $V_s = -1$ and the standard set of parameters stated in the text. In the figure, the broken, dotted, and solid curves refer to the field emission, usual emission, and total flux, respectively, while the color labels of the varying parameter s are indicated on the curves.

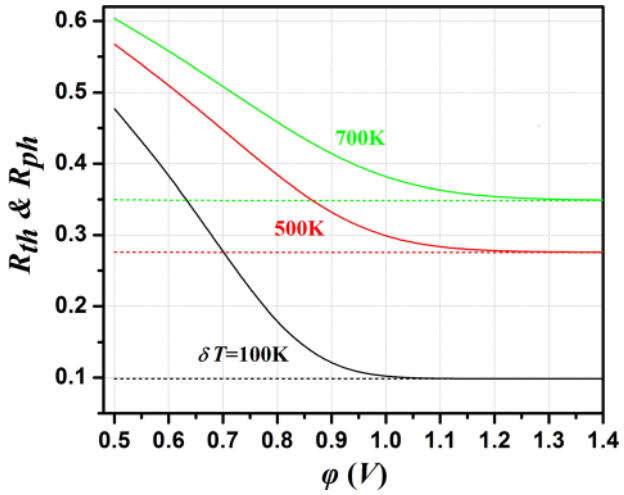

FIG. 5. The ratio of currents (R_{th} and R_{ph}) as a function of the work function φ (or the barrier height W_a) from the graphene sheet for different values of parameter δT for $V_s = 0.1$ and the standard set of parameters stated in the text. In the figure, the broken and solid curves refer to the emission flux associated with thermionic (R_{th}) and photoelectric (R_{ph}) effects, respectively, while the color labels of the varying parameter δT are indicated on the curves.

negative surface potential; this nature can be understood in terms of large electron population for tunneling (between energy range ϵ (0, $W_a - V_s$)) and sharper barrier. However, the ratio was noticed to decrease with increasing surface temperature (δT), but this is due to enhanced current from the uncharged surface; in terms of magnitude, the emission current increases with surface temperature. The effect of positively charged surfaces is illustrated in Fig. 2(b), where the ratio (and hence the emission flux) is seen to decay with increasing surface potential; this nature may be attributed to the increase in the barrier height of the quantum well for the electron emission as ($W_a + V_s$). The effect of different δT values may be understood in terms of the high energy electron population available for the emission in the tail of the distribution, which is shortened in the presence of the positive potential barrier (V_s) over the surface. Following the distribution function (f_{de}), the population density (n) at large operating temperature may be approximated as $n \propto \exp[-(\varepsilon - \varepsilon_f + \upsilon_s)]$. Using this, the population density of electrons with respect to an uncharged surface ($V_s = 0$) may be expressed as $n/n_0 = \exp(-V_s/kT)$. This estimate clearly shows that the difference in the electron population in three cases, viz., $\delta T = 700$, 500, and 300 K, is more pronounced for moderate $V_s \epsilon$ (0.05, 0.3) V values.

The effect of varying surface temperature ($T = T_o + \delta T$, which effectively manifests the laser and material properties) on the current ratios (R_{th} and R_{ph}) has been displayed in Fig. 3 for different values of surface potential; the behaviour is similar to that discussed in Fig. 2. The influence of the electric field span (depicted by s as electric field strength $f = V_s/s$), which ultimately affects the tunneling probability [$T(\varepsilon_x)$, Eq. (8)] and hence the field emission for $V_s = -1.0$V, has been displayed in Fig. 4. The ratios (R_{th} and R_{ph}) and hence the emission flux are observed to increase with decreasing s; this nature is primarily a consequence of the sharper barrier for tunneling due to increasing electric field strength, and it

literally reciprocates the effect similar to increasing V_s (Figs. 2 and 3). As indicated, the work function of graphene may significantly be tuned via the surface engineering/morphology, and the effect of varying φ on the emission current from positively charged surfaces ($V_s > 0$) for three different values of δT is illustrated in Fig. 5. An arbitrary value of the surface potential (*say* $V_s = 0.1$V) corresponding to the pristine graphene is chosen for the illustration purpose; however, this parameter may also be tuned via adjusting the work function/surface barrier by the surface morphology. The broken curves refer to the ratio corresponding to thermionic flux (R_{th}), while the solid lines correspond to photoelectric flux (R_{ph}). It is observed that the ratios for the two currents deviate from each other for the small work function values; this nature is primarily a consequence of the enhanced electron population available for the emission inside the surface in the case of laser illumination, as the largely populated levels in the distribution shift to higher energy by $h\nu$ (~0.78 eV in present calculations).

It should be noted that the electron emitting graphene surface may acquire a finite potential depending on the physical scenario such as effective bias, effective strain, defect densities, surface morphology, and surrounding environment under consideration. For example, due to the electron emission process, a monolayer graphene sheet suspended in vacuum may acquire a finite positive potential and consequently accumulates an electron sheath in the proximity of its surface;[25] this induced potential is primarily a consequence of balance of charge flux over its surface in dynamic equilibrium. Further, the work function and corresponding surface potential may be tuned up to desired extent by taking the surface engineering into account during the fabrication process.[36] The electronic properties of the monolayer graphene can be tuned by regulating the defect density through α-beam irradiation,[37] and in this process, local distribution and induced surface potential could also be monitored. In order to establish an essence of the surface potential over monolayer graphene, the estimates for emission current corresponding to $V_s \sim 0.81\,V$ and tuned work function over a range of $\varphi \in (0.1 - 0.25)$V for different values of laser pulse power (P_L, with a spot size of $\sigma_s \sim 2.5\ \mu m^2$) along with parameters consistent with the experimental work[13] are displayed in Fig. 6. The typical value of V_s (~0.81 V) refers to the steady state equilibrium between the suspended graphene monolayer and consequent electron sheath in its proximity and has been obtained numerically by balancing the emission flux with return electron current[25] for the parameter range considered herein. In Fig. 6, the analytical estimates are displayed as the solid lines, while the bold spherical dots infer the corresponding experimental data [extracted from Fig. 4(c), Ref. 13]. As observed, the nature of the curve and quantitative estimate for the electron emission current are in reasonably good agreement with the experimental observation. The conformance of the photo-current estimates with the experimental measurements validates the applicability of the analysis and analytical expressions in the context of vertical graphene heterostructures.

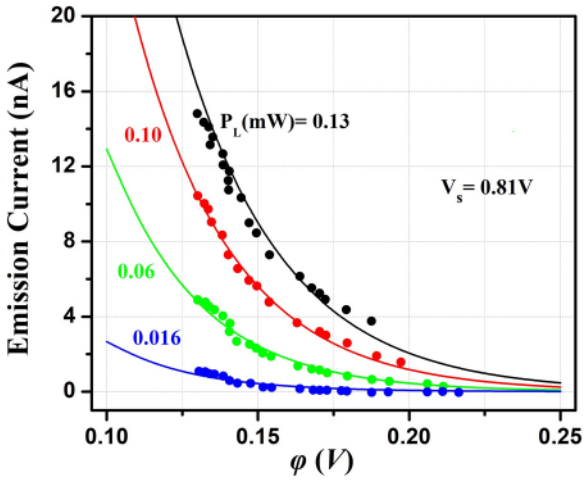

FIG. 6. The total emission (thermionic plus photoemission) current as a function of the tuned work function φ from the monolayer graphene sheet for different values of laser power (P_L with a spot size of $\sigma_s \sim 2.5\mu m^2$) and $V_s = 0.81$V along with the parameters consistent with experimental work (Ref. 13) at room temperature $T_o = 300$K; the color labels of the varying parameter P_L are indicated on the curves, while the solid spherical dots refer to the corresponding experimental data [extracted from Fig. 4(c), Ref. 13].

IV. SUMMARY AND CONCLUSIONS

Conclusively, the photon assisted electron emission from an irradiated 2D monolayer graphene sheet has been examined. The laser radiation serves a dual purpose as a finite fraction of absorbed photon energy elevates its surface temperature, causing enhanced thermionic emission of electrons, while rest of the photons lead to the photoemission at higher temperature. Following Fowler's approach of the electron emission along with the adequate density of states' configuration for the fermionic electrons (*f-d* statistics) inside the surface, a formalism describing the electron emission from an illuminated thin 2D graphene sheet has been established. On the basis of present formulation, the expressions for photon assisted field (tunneling) emission and usual emission corresponding to thermionic and photoelectric effects have been derived. Due to laser illumination, an enhancement in electron emission flux is predicted and the effect of numerous physical constituents has parametrically been examined.

The emission current is noticed to be sensitive to the parametric tuning like laser specifications, surface potential, work function, and intrinsic Fermi level; the photoemission flux is noticed to dominate over counterpart thermionic emission for lower values of the material work function, surface temperature (T), and laser wavelength (higher photon energy). As an illustrative example, for a particular set of graphene parameters ($\delta T = 70$ K, $\varphi \sim 1.0$ V, and $T_o = 400$ K) and a 0.1mW continuous laser ($\lambda \sim 1.5\,\mu$m), the enhanced flux coming out from an uncharged surface is dominated by the photoelectrons (~0.13 A/cm^{-2}) in comparison to the thermionic current (0.18 mA/cm^{-2}). Further, considering the possibility of fine tuning of the surface barrier (work function) of the monolayer graphene to a very low value (~0.1–0.25 V) as depicted in a recent experiment,[13] the estimates for the emission current has been obtained as a function of the tuned work function and laser pulse power, which is in reasonable

agreement with the measured value. This also validates the pertinence of the analysis and analytical expressions derived herein for 2D graphene heterostructures. It is of significance to point out here that although the present analysis is performed for a 2D planar structure which takes account the linear energy dispersion, Fermionic electron population, and physical parameters (like Fermi level/work function) consistent with monolayer graphene, the formulation is certainly applicable to any arbitrary material 2D sheet. Of course, the buckling in the atomic structure having linear dispersion (e.g., silicene) may affect the intriguing electronic properties. The analysis is pertinent to the buckled atomic structures as long as the buckling (few atomic units) is considerably small in comparison to in-plane dimension. Subsequently, this analytical formulation (and expressions) may straightaway be applied to address the effect of buckling on electron emission by describing the inherent physical properties (Fermi level/work function) of buckled structures adequately, based on experimental inputs, thereby suitably tuning the parametric regime. The understanding, formulation, and current estimates of the photo-assisted electron emission from 2D sheets (layers) of advanced materials developed in this investigation may be of practical significance in improving the performance/efficiency of the energy conversion schemes for alternative power sources like photo-thermionic emitters (detectors) and converters, applicable to the power plants/industries/space assets.

ACKNOWLEDGMENTS

This work was performed under the ELI-ALPS project (GINOP-2.3.6–15-2015–00001), which was supported by European Union and co-financed by the European Regional Development fund.

[1]G. N. Hatsopoulos and E. P. Gyftopoulos, *Thermionic Energy Conversion Volume 1: Processes and Devices* (MIT Press, Cambridge, 1974).
[2]G. N. Hatsopoulos and E. P. Gyftopoulos, *Thermionic Energy Conversion Volume 2: Theory, Technology and Applications* (MIT Press, Cambridge, 1979).
[3]M. G. Kanatzidis, S. D. Mahanti, and T. P. Hogan, *Chemistry, Physics and Materials Science of Thermoelectric Materials* (Kluwer, New York, 2003).
[4]H. Xi, L. Luo, and G. Fraisse, Renewable Sustainable Energy Rev. **11**, 923–936 (2007).
[5]K. A. A. Khalid, T. J. Leong, and K. Mohamed, IEEE Trans. Electron Devices **63**, 2231–2241 (2016).
[6]S. F. Adams, AIP Conf. Proc. **813**, 590–597 (2006).
[7]G. P. Smestad, Sol. Energy Mater. Sol. Cells **82**, 227–240 (2004).
[8]J. W. Schwede, I. Bargatin, D. C. Riley, B. E. Hardin, S. J. Rosenthal, Y. Sun, F. Schmitt, P. Pianetta, R. T. Howe, Z.-X. Shen, and N. A. Melosh, Nat. Mater. **9**, 762–767 (2010).
[9]K. S. Novoselov, A. K. Geim, S. V. Morozov, D. Jiang, Y. Zhang, S. V. Dubonos, I. V. Grigorieva, and A. A. Firsov, Science **306**, 666–669 (2004).
[10]K. S. Novoselov, A. K. Geim, S. V. Morozov, D. Jiang, M. I. Katsnelson, I. V. Grigorieva, S. V. Dubonos, and A. A. Firsov, Nature **438**, 197–200 (2005).
[11]S. Shafraniuk, *Graphene: Fundamentals, Devices, and Applications* (Pan Stanford, Florida, 2015).
[12]W. Choi and J.-W. Lee, *Graphene: Synthesis and Applications* (CRC Press, Florida, 2016).
[13]M. Massicotte, P. Schmidt, F. Vialla, K. Watanabe, T. Taniguchi, K. J. Tielrooij, and F. H. L. Koppens, Nat. Commun. **7**, 12174 (2016).
[14]G. Pirruccio, L. M. Moreno, G. Lozano, and J. G. Rivas, ACS Nano **7**, 4810–4481 (2013).
[15]E. Gruber, R. A. Wilhelm, R. Pétuya, V. Smejkal, R. Kozubek, A. Hierzenberger, B. C. Bayer, I. Aldazabal, A. K. Kazansky, F. Libisch, A. V. Krasheninnikov, M. Schleberger, S. Facsko, A. G. Borisov, A. Arnau, and F. Aumayr, Nat. Commun. **7**, 13948 (2016).
[16]L. Zhang, Y. Yan, H. C. Wu, D. Yu, and Z. M. Liao, ACS Nano **10**, 3816–3822 (2016).
[17]R. Bistritzer and A. H. MacDonald, Phys. Rev. Lett. **102**, 206410 (2009).
[18]K. J. Tielrooij, J. C. W. Song, S. A. Jensen, A. Centeno, A. Pesquera, A. Zurutuza Elorza, M. Bonn, L. S. Levitov, and F. H. L. Koppens, Nature Phys. **09**, 248–252 (2013).
[19]N. W. Ashcroft and N. D. Mermin, *Solid State Physics* (Harcourt College Publishers, New York, 1976).
[20]R. H. Fowler, *Statistical Mechanics: The Theory of the Properties of Matter in Equilibrium* (Cambridge University Press, London, 1955).
[21]P. R. Wallace, Phys. Rev. **71**, 622–634 (1947).
[22]S.-J. Liang and L. K. Ang, Phys. Rev. Appl. **3**, 014002 (2015).
[23]F. Seitz, *Modern Theory of Solids* (Mc Graw Hill Book Co., New York, 1940).
[24]A. H. C. Neto, F. Guinea, N. M. R. Peres, K. S. Novoselov, and A. K. Geim, Rev. Mod. Phys. **81**, 109–162 (2009).
[25]S. Misra, M. U. Kahaly, and S. K. Mishra, J. Appl. Phys. **121**, 065102 (2017).
[26]Z. Jiang, E. A. Henriksen, L. C. Tung, Y.-J. Wang, M. E. Schwartz, M. Y. Han, P. Kim, and H. L. Stormer, Phys. Rev. Lett. **98**, 197403 (2007).
[27]Y. Yin, Z. Cheng, L. Wang, K. Jin, and W. Wang, Sci. Rep. **4**, 5758 (2014).
[28]M. S. Sodha, *Kinetics of Complex Plasmas* (Springer, New Delhi, 2014).
[29]S. K. Agarwal, S. Misra, S. K. Mishra, and M. S. Sodha, Can. J. Phys. **90**, 265–275 (2012).
[30]S. K. Mishra, M. S. Sodha, and S. Misra, Phys. Plasmas **19**, 073705 (2012).
[31]M. S. Sodha and S. K. Mishra, "Lunar photoelectron sheath and levitation of dust," Phys. Plasmas **21**, 093704 (2014).
[32]S. Misra, S. K. Mishra, and M. S. Sodha, Phys. Plasmas **22**, 043705 (2015).
[33]A. Ghatak and S. Loknathan, *Quantum Mechanics: Theory and Applications* (Springer Science + Business Media, Dordrecht, 2004).
[34]M. S. Sodha and S. K. Mishra, Phys. Plasmas **18**, 044502 (2011).
[35]E. Starodub, N. C. Bartelt, and K. F. McCarty, Appl. Phys. Lett. **100**, 181604 (2012).
[36]H. Yuan, S. Chang, I. Bargatin, N. C. Wang, D. C. Riley, H. Wang, J. W. Schwede, J. Provine, E. Pop, Z. X. Shen, P. A. Pianetta, N. A. Melosh, and R. T. Howe, Nano Lett. **15**, 6475–6480 (2015).
[37]J. H. Kim, J. H. Hwang, J. Suh, S. Tongay, S. Kwon, C. C. Hwang, J. Wu, and J. Y. Park, Appl. Phys. Lett. **103**, 171604 (2013).